Proceedings of the
International Conference on Mechanical Engineering and Renewable Energy 2013
(ICMERE2013) 1 – 3 May 2014, Chittagong, Bangladesh

ICMERE2013-PI-290

MONOTONIC AND CYCLIC RESPONSES OF A FERRITIC STAINLESS STEEL FOR THE APPLICATION OF HIGH-TEMPERATURE STRUCTURE

S M Humayun Kabir[1,*], **Tae-in Yeo**[2] **and M Aman Ullah**[3]

[1, 3] Department of Mechanical Engineering,
Chittagong University of Engineering and Technology, Chittagong-4349, Bangladesh.
[2] School of Mechanical and Automotive Engineering,
University of Ulsan, P.O. Box 18 Ulsan 680-749, Republic of Korea.

[1,*]dalimuou@yahoo.com, [2]ytn@mail.ulsan.ac.kr, [3]amanctg2003@yahoo.co.in

Abstract*- In this paper, an attempt is made to evaluate the tensile and strain-controlled cyclic responses of a ferritic stainless steel which is developed for the exhaust manifold of automobiles. Here, the emphasis will be placed on the temperature effect on tensile properties such as yield strength and ultimate tensile strength. Moreover, the objective of this study is also to reveal the mixed mode of cyclic hardening–softening behavior of the ferritic stainless steel under the fatigue test conditions. A parameter, critical accumulated plastic strain, is introduced to the constitutive equations for the material for describing the hardening - softening responses. The nonlinear constitutive equations for describing the cyclic responses are implemented into Finite Element code using determined parameters for obtaining numerical simulation. The stabilized hysteretic responses obtained from experiment and predicted from numerical simulation are compared and found to be realistic.*

Keywords: Ferritic stainless steel, Monotonic response, Cyclic hardening/softening, Accumulated plastic strain, Finite element code.

1. INTRODUCTION

Many engineering components experience cyclic loadings under isothermal and anisothermal conditions during their service life, such as exhaust manifold systems of automobile, wheels in railroad industry, pressure vessels in chemical or power plants, and so on. Now-a-days, increased operating temperature is very common for improved performance in high-temperature structure. Consequently, the properties, such as light weight, high corrosion resistance, and fairly high thermal fatigue resistance are of greater importance in selection of material for high temperature-structure such as in exhaust manifold systems of automotives. So the material parameters and mechanical properties of structural steels in elasto-plastic cyclic behavior have gained interests in many studies during recent years to replace cast iron, the traditional material for this application [1-5]. For years, various theoretical constitutive models based on continuum mechanics have been developed for describing the material nonlinearities and allowing accurate modeling of hardening/softening responses under cyclic loading conditions [6-9]. And, characterization of material parameters are important research concerning accurate presentation of inelastic responses of engineering components.

Even though austenitic stainless steel has better strength at elevated temperatures than ferritic stainless steel, the use of ferritic stainless steel has also been increased due to its excellent corrosion resistance, moderate thermal fatigue resistance, and low prices. In this study, monotonic tensile and strain-controlled low cycle fatigue results are investigated on a ferritic stainless steel which is developed for the exhaust manifold used in exhausts system of automobiles. This study analyzes the influence of temperature and strain amplitude on monotonic and cyclic responses over a wide range of temperatures. Thereafter, a presentation of the temperature effect on tensile properties of the material, description of the mixed mode of Cyclic hardening–softening behavior of the material under the fatigue test conditions, an introduction of critical accumulated plastic strain to the constitutive equations for describing the cyclic hardening - softening responses of the material, determination of material parameters of constitutive equations and a brief description of the simulation of the adopted constitutive equations utilizing the determined parameters, and comparison of analysis results with those of the experimental stabilized hysteresis loops at different temperatures are presented in subsequent sections.

2. MATERIALS AND EXPERIMENTAL RESULTS

In this study, tensile and strain-controlled low cycle fatigue data of a 400-series ferritic stainless steel designated as SS400-C over a wide range of temperature is employed to examine the material responses. Nominal chemical compositions of studied ferritic stainless steel are shown in Table 1. The specimens used in this study are fabricated with the required surface preparation in accordance with ASTM Standard E606. A closed-loop

Table 1. Chemical composition of the ferritic stainless steel (wt%).

C	Si	P	S	Cr	Mn	Mo	Nb
0.025	1.00	0.04	0.03	17.00	1.00	1.12	0.60

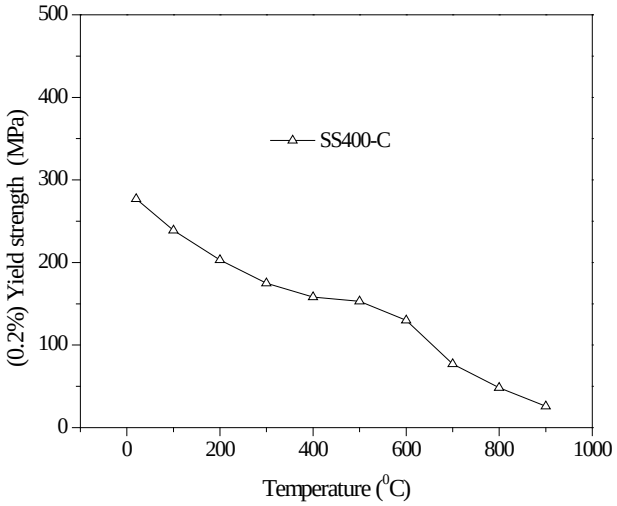

Fig. 1: Temperature dependent mechanical properties (Yield strength).

servo-hydraulic test system with 10-ton capacity manufactured by MTS is used to conduct all tests. The strain rate is maintained in a constant value of 2×10^{-3} /s to reduce the influences of strain rate. The waveform is triangular. The strain amplitudes and stress amplitudes are determined at stabilized loop of each specimen.

2.1 Monotonic Tensile Responses

The influence of temperature on yield strength and ultimate tensile strength (UTS) are examined which show that material strengths decrease with increasing temperature. It can be seen through Fig. 1 and Fig. 2 that in temperature region 200^0C-500^0C, the reduction of yield strength and UTS are retarded or slightly decreased compared with other temperature regime. Fig.3 demonstrates the serration [11] of tensile stress-strain curve of SS400-C where it is evident that serrated flow is well-defined in the temperature regime of 200^0C-600^0C. Finally, considering plateau in the variation of yield strength and UTS and pronounced serrated flow the temperature regime of 200^0C-500^0C can be defined as dynamic strain ageing [12-13] regime for the considered ferritic steels in terms of monotonic loading conditions. Hong and Lee [14] observed the similar phenomena of dynamic strain ageing (DSA) for a carbon steel with different temperature range. DSA can be considered effective in strengthening steels when an anomaly appears in the flow stress vs temperature dependence. But DSA has deteriorating effect on fatigue life [15-18].

2.2 Isothermal Cyclic Deformation Behavior and Peak Stress Evaluation

Temperature and strain amplitude affect the cyclic deformation behavior of materials significantly. Fig.4 and Fig. 5 are the typical representation of the influence

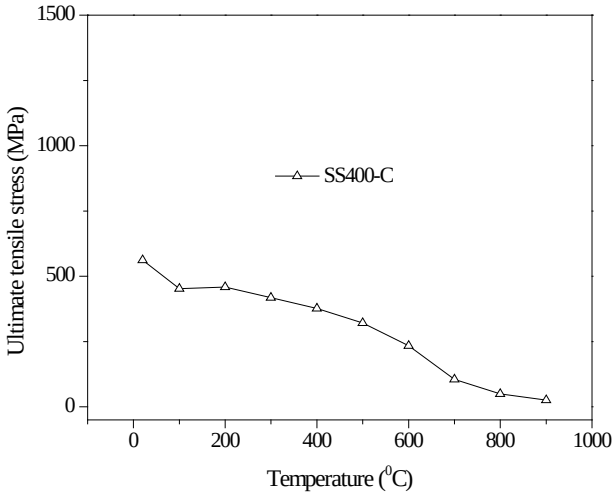

Fig. 2: Temperature dependent mechanical properties (Ultimate tensile stress).

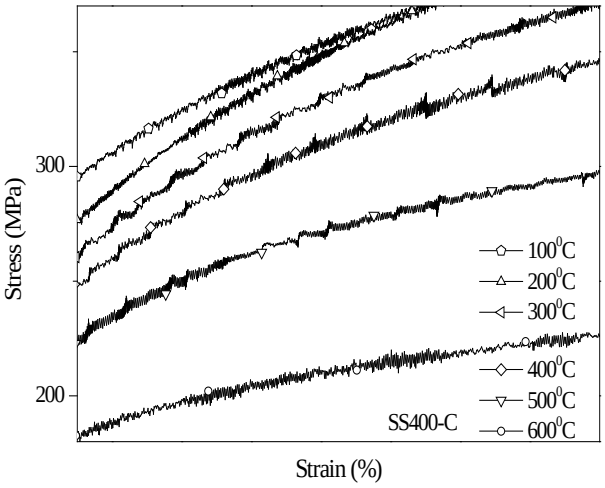

Fig. 3: Segment of tensile stress-strain curves shows serrated flow.

of strain amplitude and temperature on the evolution of peak stress versus applied cycles for the material SS400-C. Figure 4 depicts that the peak stresses increase with the increasing strain amplitude. These figures indicate that SS400-C exhibits initial cyclic hardening for nearly first 10 cycles followed by cyclic softening during most of the fatigue life for the temperature range RT~400^0C. But at 500^0C and 600^0C, the cyclic hardening phenomena are dominant throughout the low cycle fatigue life. Kruml and Pola'k [19] and Pola'k et al. [20] noticed the similar mixed mode of Cyclic hardening–softening phenomena in case of X10CrAl24 and 446 ferritic stainless steels respectively. Cyclic softening in ferritic steel was also found in other literatures [21-23]. An important feature of the cyclic straining of polycrystalline materials is the redistribution of the cyclic plastic strain and its localization. The increase of dislocation density caused by strain cycling leads to decrease in dislocation mobility; hence hardening occurs usually.

Kruml et al.[19] reported that high density of screw dislocations from several slip systems is produced within

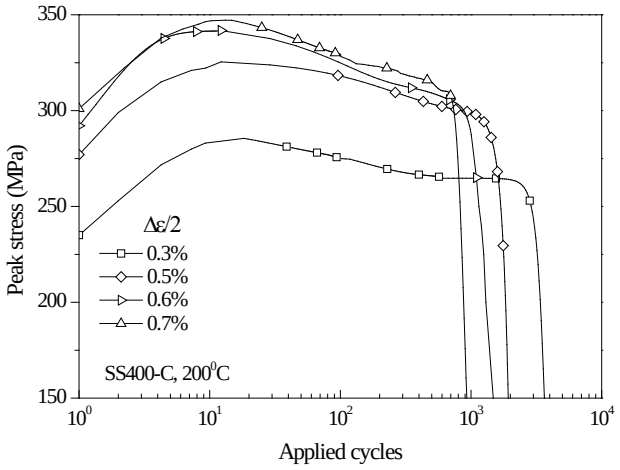

Fig. 4: Influence of strain amplitude on the evolution of peak stress of SS400-C at 200^{0}C.

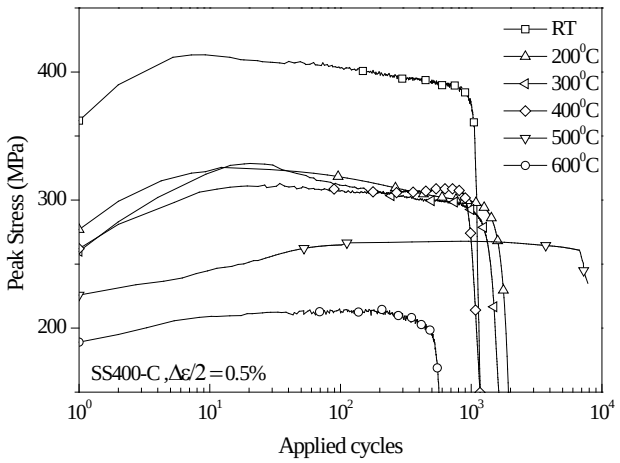

Fig. 5: Influence of temperatures on evolution of peak stress of SS400-C at $\Delta\varepsilon/2 = 0.5\ \%$

first few cycles, and no rearrangement to the spatial dislocation structures were found in the majority of grains when examined a ferritic steel. It was also reported that the redistribution of the cyclic plastic strain and its localization is the source of cyclic softening at the later stage of life. Shankar et al. [24] also stated that initial hardening could results from combination of formation of fine precipitates on dislocations during testing and DSA as a consequence of interaction between dislocations and solute atoms. Therefore, it is reasonable to be believed that the initial hardening of the present material could result from either individual or combined effects of (i) mutual interaction among dislocations and (ii) formation of fine precipitates on dislocations during testing, and (iii) DSA. And, cyclic softening can be related to the localization of the cyclic plastic strain into the bands of intensive cyclic slip. The typical stabilized hysteresis loops at different strain amplitude (0.3% ~ 0.7%) are translated to the lower peak in Fig. 6 for the temperature of 200C. Figure 6 indicates that magnitude of the stabilized stress increases with the increase of strain amplitude for a particular temperature.

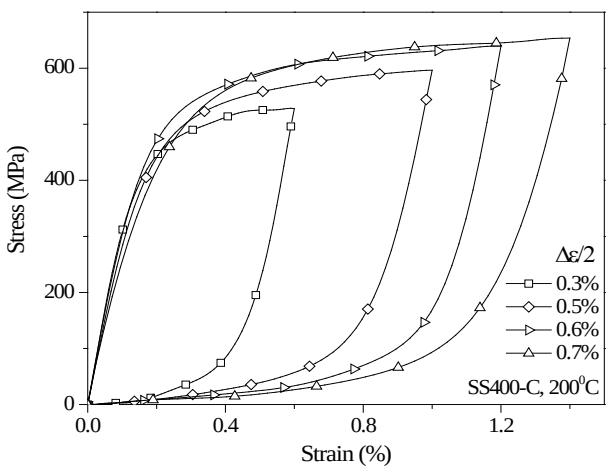

Fig. 6: Stabilized hysteresis loops of SS400-C adjusted to the lower peak.

3. CONSTITUTIVE EQUATIONS

For stainless steel, it is well recognized that materials undergo through cyclic hardening or cyclic softening. If, in addition to the kinematic hardening, the material also isotropically hardens or softens, then superimposed upon the translation of yield surface is a progressive expansion or contraction. Within an individual cycle, kinematic hardening is the dominant hardening process, but over a large number of cycles the materials also hardens or softens isotropically such that peak stress and strain in a hysteresis loop increase or decrease from one cycle to the next until saturation is achieved. This process is often called cyclic hardening/softening. The amount of expansion or contraction of yield surface is often taken to be a function of accumulated plastic strain p [25],

$$p = \int dp \tag{1}$$

with the increment in accumulated plastic strain $dp = \sqrt{(2/3)(d\boldsymbol{\varepsilon_p} : d\boldsymbol{\varepsilon_p})}$, where $\boldsymbol{\varepsilon}_p$ is the plastic strain tensor and the operator ':' represents double contraction. Constitutive model defines the material stress-strain relationship. The rate independent plasticity models considered in this study have the following common features:

i) von-Mises yield criterion (yield surface): The elastic domain is defined by [25],

$$f\left(\boldsymbol{\sigma} - \alpha\right) = \boldsymbol{J}\left(\boldsymbol{\sigma}' - \alpha'\right) - \sigma_y \le 0 \tag{2}$$

ii) Size of the surface,

$$\sigma_y(p) = \sigma_{y0} + r(p) \tag{3}$$

iii) The evolution of isotropic variable [8, 10],

$$dr = b(Q - r)dp \tag{4}$$

iv) The evolution of kinematic hardening variable [10],

$$d\alpha = \frac{2}{3} C d\boldsymbol{\varepsilon}_p - \gamma\alpha dp \tag{5}$$

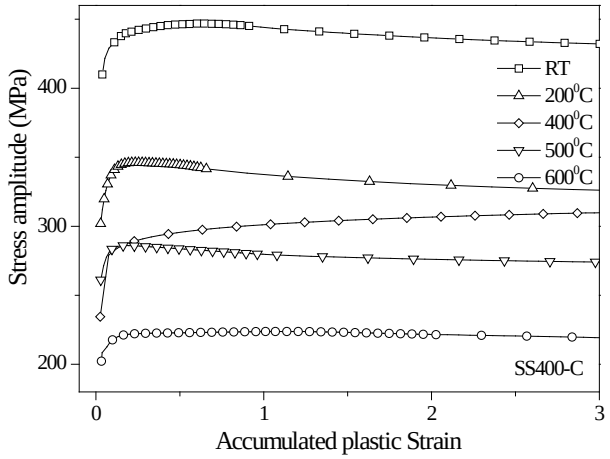

Fig. 7: Experimental $\Delta\sigma/2-p$ curves of SS400-C at different temperatures.

where, $\boldsymbol{\sigma}'$ is the deviatoric part of stress tensor $\boldsymbol{\sigma}$, α is the current center of the yield surface in total stress space (back stress tensor) and α' is the deviatoric part of back stress tensor, f is the yield function, $J(\cdot)$ represents von-Mises invariant, σ_y is the size of the yield surface which takes into account the initial yield size σ_{y0} and isotropic function r, σ_{y0} is the initial size of the surface with $r(0)=0$, Q is the stabilized value of r, constant b controls the pace of the isotropic hardening, and C and γ are material constants regarding kinematic hardening.

For the material SS400-C, Fig. 7 shows that stress increases with respect to cycles up to the stabilization at 400^{0}C but stress increases for a first few cycles and decreases up to the stabilization state for other temperatures. Due to mixed mode of evolution of stress with respect to cycles, using Eq.(4) two isotropic variables with a p_{cr} is introduced in this study for the evolution of isotropic variable in the following manner,

$$r = Q_1(1-e^{-b_1 p}) - HVF\left(p-p_{cr}\right)[Q_2(1-e^{-b_2(p-p_{cr})})] \tag{6}$$

with the following two criteria

$$\begin{aligned} &if\ \ p_{cr}\neq 0\ \ and\ \ \left(p-p_{cr}\right)>0\ \ then\ HVF(\cdot)=1 \\ &\qquad\qquad \left(p-p_{cr}\right)<0\ \ then\ HVF(\cdot)=0 \end{aligned} \tag{7}$$

and

$$if\ \ p_{cr}=0\ \ and\ \ \left(p-p_{cr}\right)>0\ \ then\ HVF=-1 \tag{8}$$

where, in Eq.(6), the first isotropic variable r_1 is,

$$r_1 = Q_1(1-e^{-b_1 p}) \tag{9}$$

and second isotropic variable r_2 is,

$$r_2 = Q_2(1-e^{-b_2(p-p_{cr})}) \tag{10}$$

and p_{cr} is the critical accumulated plastic strain above which second isotropic variable works. Q_1 and Q_2 represent the asymptotic values of the isotropic variables r_1 and r_2 respectively. b_1 and b_2 represent the stabilization curve steepness for the isotropic variables r_1 and r_2 respectively. First isotropic variable represents the cyclic hardening and second isotropic variables demonstrates the cyclic hardening or softening depending upon the above two criteria. Therefore, p_{cr} controls the mode of cyclic response which is a function of temperature for particular strain amplitude. Therefore, p_{cr} controls the mode of cyclic response which is a function of temperature for particular strain amplitude.

4. ANALYSIS

In this section, extraction of material parameters and how the constitutive equations are implemented into finite element simulation are stated in a brief. The simulation results are also compared with that of the experiment.

4.1 Material Parameters

Considering that low cycle fatigue failure occurs usually after several hundreds of load cycles, the parameters are calibrated using the stabilized loops. The plastic parameters are determined with the available strain-controlled cyclic tests data from at isothermal condition. Correlating between the two models [26] in terms of their parameters, determination of hardening parameters is done systematically and efficiently for structural steels which either cyclically harden or soften. In this approach [26], the critical accumulated plastic strain p_{cr} is introduced which controls the mode of cyclic responses depicted in Fig. 4 and Fig. 7. The critical accumulated plastic strain is calculated easily first at $\Delta\varepsilon/2=0.7\ \%$ for different temperature from Fig.7. Then, isotropic parameters Q_1, Q_2, b_1, and b_2 are determined. Utilizing the concept of stabilized elastic limit [26], the Young's modulus is derived directly from the linear part of the stabilized hysteresis loop (Fig. 6) which is denoted here as E^*. After determination of isotropic parameters kinematic hardening parameters are determined. Utilizing stabilized hysteresis loop data with the built-in calibration procedure of the ABAQUS code, C and γ of kinematic hardening variable are determined. Detail procedure for determining the material parameters can be found elsewhere [26]. The determined parameters for different materials are listed in Table 2 and Table 3.

Table 2: Isotropic Parameters with p_{cr} at $\Delta\varepsilon/2=0.7\ \%$.

Temp. ^{0}C	E^* (GPa)	σ_{y0} (Mpa)	Q_1 (Mpa)	Q_2 (Mpa)	b_1	b_2	p_{cr}
RT	269	219	37	21	9.4	0.50	0.631
200	206	189	47	30	17	0.51	0.308
400	144	134	53	22	16	1.10	0.000

Table 3: Kinematic hardening parameters at $\Delta\varepsilon/2 = 0.7$ %

Temp. ^{0}C	C (MPa)	γ
RT	140788.00	869.53
200	54667.97	599.41
400	67297.59	736.43

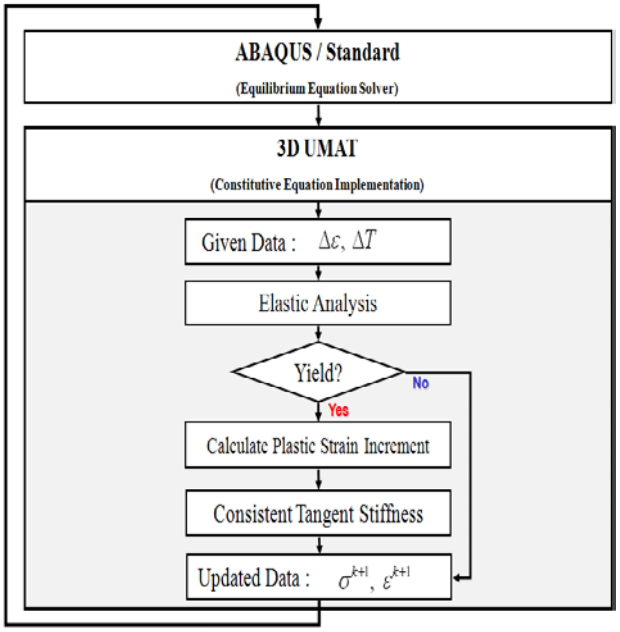

Fig. 8: Incorporation of UMAT with ABAQUS.

4.2 Numerical Simulation and Results

For numerical simulation, the resulting discretized equations for the non-linear constitutive equations mentioned in section 3 are summarized as follows [26],

$$ {}^{n+1}f = \sqrt{\frac{3}{2}}\left|{}^{n+1}\boldsymbol{\tau}^{\mathrm{tr}}_{\mathrm{dev}}\right| - (3G + {}^{n+1}\Phi C)\Delta p - {}^{n+1}r(\Delta p) - \sigma_{y0} = 0 \qquad (11) $$

with

$$ {}^{n+1}\boldsymbol{\tau}^{\mathrm{tr}}_{\mathrm{dev}} = {}^{n+1}\boldsymbol{\sigma}^{\mathrm{tr}'} - {}^{n+1}\Phi\ {}^{n}\alpha' \qquad (12) $$

In this implicit scheme, the index $n+1$ represents the current time step. If the material is in the plastic region then the unknown variable Δp is to be solved out. Then, the stress, accumulated plastic strain, and other variables are updated and a new strain increment is taken. In Eq.(11) , isotropic variable r is evolved according to the Eq. (6) depending upon the criteria associated with the critical accumulated plastic strain p_{cr} .

The nonlinear constitutive equations are implemented into Finite Element (FE) code through ABAQUS by means of a UMAT (User subroutine to define a MATerial's mechanical behavior) subroutine. The incorporation of UMAT in ABAQUS works as in

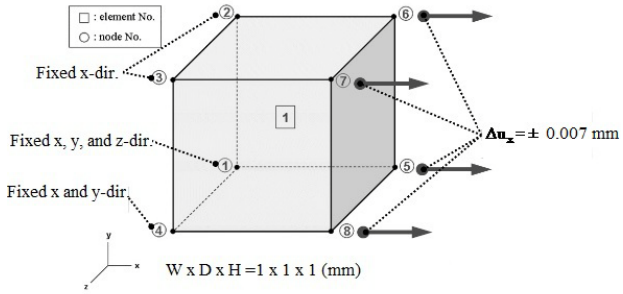

Fig. 9: Boundary Conditions for finite element analysis.

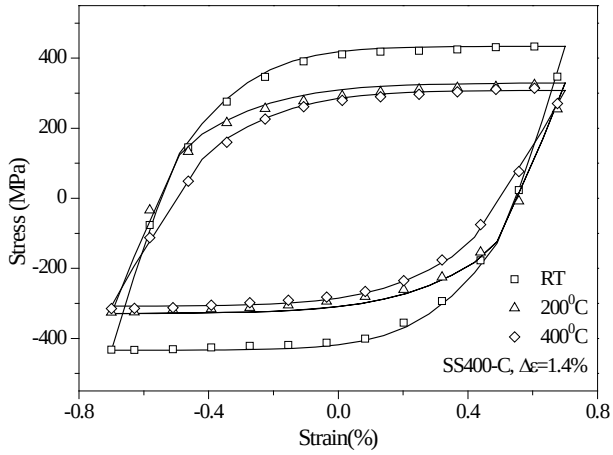

Fig. 10: Comparisons of stabilized hysteresis loops for SS400-C (Solid Lines: Simulation results, Symbols: Experimental data).

Fig.8. In FE simulation, only one finite element, in the middle of the sample, is submitted to an imposed strain $\Delta\varepsilon/2 = \pm 0.007$ and subsequently analysis is carried out. The proper boundary condition imposed on the element is described graphically in Fig. 9.

The experimental results of stabilized hysteresis loops together with UMAT results for the material considered are in Fig. 10 The prediction of stabilized loops coincides well with the experimental results. Comparisons reveal that incorporation of critical accumulated plastic strain are said to be reasonable to represent mixed mode of evolution of stress (hardening and softening) for the material considered.

5. CONCLUSION

Inelastic responses of a ferritic stainless steel are carefully experimentally studied under tensile monotonic and low cycle fatigue tests. Several tests have been performed to derive the basic data. Tests results have shown a strong influence of temperature and strain amplitude on monotonic responses as well as on low cycle responses. Under monotonic tensile test, anomalous dependence of flow stress with temperature and serrations in stress-strain curves are believed to be manifestations of DSA. The material displays mixed mode of hardening and softening behavior at different temperatures when the material is subjected to cyclic loadings and the peak stresses increase with the

increasing strain amplitude. An attempt is made to introduce the critical accumulated plastic strain above which second isotropic variable works for describing mixed mode of cyclic responses. For comparison purpose, constitutive equations are implemented into finite element simulation considering mixed mode of cyclic hardening-softening. It is noteworthy that the simulation results with determined material parameters predict well the experimental stabilized loops at different temperatures.

6. ACKNOWLEDGEMENT

The authors express their thanks to SEJONG INDUSTRIAL CO. LTD., Republic of Korea for the support in acquiring of the material data.

7. REFERENCES

[1] N. Fujita, K. Ohmura, M. Kikuchi, T. Suzuki, S. Funaki, and I. Hiroshige, "Effect of Nb on high-temperature properties for ferritic stainless steel ", *Scripta Materialia* , vol. 35, pp. 705-710, 1996.

[2] J. Beddos and J. G. Parr, *Introduction to stainless steels*, 3rd edition, ASM Intl, 1998.

[3] V. Shankar, M. Valsan, R. Kannan, K.B.S. Rao, S.L. Mannan, and S.D. Pathak, "Low cycle fatigue behavior of a modified 9Cr-1 Mo Ferritic steel", *ISRS on Material Science and Engineering*, Chennai, India, 2004.

[4] K. O. Lee, S. Yoon, S. B. Lee and B. S. Kim, Low cycle fatigue behavior of 429EM ferritic steel at elevated temperatures, *Key Engineering Material*, 261-263 (2004) 1135-1140.

[5] M. Avalos, I. Alvarez-Armas, and A. F. Armas, "Dynamic strain aging effects on low-cycle fatigue of AISI 430F", Materials Science and Engineering: A, vol. 513-514, pp. 1-7, 2009.

[6] P. J. Armstrong and C.O. Frederick, "A mathematical representation of the multiaxial Bauschinger effect", G.E.G.B. Report RD/B/N, pp. 731-747, 1966.

[7] Y. F. Dafalias and E.P. Popov, "Plastic internal variables formalism of cyclic plasticity", *Journal of Applied Mechanics*, vol. 43, pp. 645-650, 1976.

[8] J. L. Chaboche, "Time-independent constitutive theories for cyclic plasticity", *International Journal of Plasticity*, vol. *2*, n. 2, pp. 149-188, 1986.

[9] D. Y. Chiang and J. L. Beck, "A new class of distributed-element models for cyclic plasticity-I. Theory and applications", *International Journal of Solids and Structures*, vol. 31, pp. 469-484, 1994.

[10] J. L. Chaboche, "A review of some plasticity and viscoplasticity constitutive theories", *International Journal of Plasticity*, vol. 24, pp. 1642–1693, 2008.

[11] P. Rodriguez, "Serrated plastic flow", *Bulletin of Material Science*, vol. 6, no. 4, pp. 653-663, 1984.

[12] .A. H. Cottrell and B**.** A. Bilby, "Dislocation Theory of Yielding and Strain Ageing of Iron", Proceedings of the Physical Society A, XII, pp. 49-62, 1949.

[13] L.P. Kubin and Y. Estrin, "Dynamic strain ageing and mechanical response of alloys", *Journal of Physics III* , vol., no. 6, pp. 929-943, 1991.

[14] S. G. Hong, and S. B. Lee, "Influence of strain rate on tensile and LCF properties of prior cold worked 316L stainless steel in dynamic strain aging regime", *Fatigue Damage Materials: Experiment and Analysis*, WIT press, pp.137-147, 2003.

[15] H. Abdel-Raouf, A. Plumtree, and T.H. Topper, "Effects of temperature and deformation rate on cyclic strength and fracture of low carbon steel", ASTM STP 519, pp. 28-57, 1973.

[16] J. Bressers, "High temperature alloys, their exploitable potential", J.B. Marriott, M. Merz, J. Nihoul, J. Ward, editors, Elsevier Applied Science, pp. 385-410, 1987.

[17] V.S. Srinivasan, R. Sandhya, M. Valsan, K. B.S. Rao, S.L. Mannan and D.H. Sastry., The influence of dynamic strain ageing on stress response and strain-life relationship in low cycle fatigue of 316L(N) stainless steel, *Scripta Materialia*, vol. 37, no. 10, pp. 1593-1598, 1997.

[18] S.-G. Hong, S.-B. Lee, "The tensile and low-cycle fatigue behavior of cold worked 316L stainless steel: influence of dynamic strain aging", *International Journal of Fatigue*, vol. 26, pp. 899-910, 2004.

[19] T. Kruml and J. Pola´k, "Fatigue softening of X10CrAl24 ferritic steel", Materials Science and Engineering: A, vol.319–321 , pp.564–568, 2001.

[20] J. Pola´k , F. Fardoun, and S. Degallaix, "Analysis of the hysteresis loop in stainless steels I. Austenitic and ferritic steels", Material Science and Engineering: A, vol. 297, pp.144-153, 2001.

[21] K. Pohl, P. Mayr, and E. Macherauch, "Cyclic deformation behavior of a low carbon steel in the temperature range between room temperature and 850K", *International Journal of Fracture*., vol.17, pp.221-233, 1981.

[22] H. J. Roven and E. Nes, "Cyclic deformation of ferritic steel: I. Stress–strain response and structure evolution", Acta Metallurgica et Materialia, vol. 39, pp.1719-1733, 1991.

[23] T. Petersmeier, U. Martin, D. Eifler, and H. Oettel, "Cyclic fatigue loading and characterization of dislocation evolution in the ferritic steel X22CrMoV121", International Journal of Fatigue, vol. 20, pp. 251-255,1998.

[24] V. Shankar, M. Valsan, R. Kannan, K.B.S. Rao, S.L. Mannan, and S.D. Pathak, "Low cycle fatigue behavior of a modified 9Cr-1 Mo Ferritic steel", *ISRS on Material Science and Engineering*, Chennai, India, 2004.

[25] F. Dunne and N. Petrinic, *Introduction to computational plasticity* ,Oxford University Press, 2005.

[26] S. M. H. Kabir and T. Yeo, "Characterization of unified material parameters in elasto-plastic continuum approach", *International Review of Mechanical Engineering*, vol. 4, no. 5, pp. 507-517, 2010.

8. NOMENCLATURE

Symbol	Meaning
$\boldsymbol{\sigma}$	Stress tensor
$\boldsymbol{\sigma}'$	Deviatoric part of stress tensor
σ_y	Size of the yield surface
σ_{y0}	Initial size of the surface
α	Back stress tensor
α'	Deviatoric part of back stress tensor
$\Delta\sigma/2$	Stress amplitude
$\Delta\varepsilon/2$	Strain amplitude
$\boldsymbol{\varepsilon_p}$	Plastic strain tensor
$d\boldsymbol{\varepsilon_p}$	Increment of plastic strain tensor
$\boldsymbol{J}(\cdot)$	von-Mises invariant
b_1	The rate of saturation of r_1
b_2	The rate of saturation of r_2
C , γ	Kinematic hardening parameters
f	Yield function
Δp	Increment of accumulated plastic strain
p_{cr}	Critical accumulated plastic strain
Q_1	Saturated value of
Q_2	Saturated value of
r	Isotropic hardening function
r_1, r_2	Isotropic hardening functions
${}^{n+1}\Phi$	$1/(1+\gamma\Delta p)$
${}^{n+1}\boldsymbol{\sigma}^{\mathrm{tr}'}$	Deviatoric Trial Stress
:	Double contraction